The Astrophysical Journal, 999:206 (12pp), 2026 March 10 https://doi.org/10.3847/1538-4357/ae433e

Comparative Analysis of Properties of Coronal Mass Ejections at High and Low Apparent Latitudes in 1996–2025

Olga Khabarova[1], Nuran Samara[2,3], Noam Tishler[2], Hadar Reshef[2], and Colin Price[2]
[1] Interdisciplinary Centre for Security, Reliability and Trust, University of Luxembourg, Luxembourg; olga.khabarova@uni.lu
[2] Department of Geophysics, Tel Aviv University, Ramat Aviv, Tel Aviv, Israel
[3] Department of Social Sciences, Tel Aviv University Ramat Aviv, Tel Aviv, Israel
Received 2024 August 20; revised 2026 February 6; accepted 2026 February 7; published 2026 March 5

Abstract

This study examines the statistical properties of coronal mass ejections (CMEs) over two and a half solar cycles (1996–2025) using coronal observations from the SOHO LASCO CDAW and CACTus catalogs, supplemented by sunspot number records and in situ measurements of interplanetary CMEs (ICMEs) from the Ulysses spacecraft. Focusing on differences between CMEs originating at different apparent latitudes (AL), we analyzed CME annual rates, spatial distributions, and kinematic properties. The total yearly number of CMEs follows the solar cycle, with high-AL CMEs showing a stronger link than low-AL ones. A pronounced solar-cycle-dependent variation is observed between the number of CMEs detected in the corona and the ICMEs in the solar wind. During solar maximum, ICME counts are substantially lower than coronal ejection rates, likely due to enhanced deflection and interaction in the complex interplanetary medium, whereas during solar minimum, Ulysses captured several times more high-latitude ICMEs. ICME occurrence at Ulysses follows the solar cycle with a systematic two-year phase lag. Spatially, high-AL CMEs display a south–north asymmetry, being preferentially directed northward across all phases of the solar cycle except the solar maximum. Low-AL CMEs show a slight southward bias at solar maximum. During the rising phase, they are northward on the western side and southward on the eastern side, with the opposite pattern in the declining phase. The linear speed and angular width of both low- and high-AL CMEs track the solar cycle, with the CME angular width variations preceding sunspot activity, which suggests potential prognostic applications.

Unified Astronomy Thesaurus concepts: Solar coronal mass ejections (310); Heliosphere (711)

1. Introduction

Studies in space physics prioritize coronal mass ejections (CMEs) and their interplanetary counterparts (ICMEs) as crucial objects of investigation. An obvious reason for that is that ICMEs are known as effective drivers of geomagnetic storms, which requires understanding properties of CMEs in the corona and evolution of these sources of the high-speed solar wind and the compressed turbulent plasma in the ICME sheath during their propagation to the Earth (e.g., N. Gopalswamy 2016a; E. Kilpua et al. 2017; I. A. Daglis et al. 2021; D. Besliu-Ionescu & M. Mierla 2021; R. A. Howard et al. 2023). Apart from the geoeffectiveness of ICMEs, which is determined by the arrival of the enhanced ICME sheath plasma and magnetic obstacle often carrying a strong southward interplanetary magnetic field component at the Earth, ICMEs are associated with solar energetic particles, accelerated at the initial stages of the ejection development in the corona (D. V. Reames 2021). Also, significant particle acceleration at the ICME-driven shocks and the turbulent sheath region occurs locally in the solar wind, as CMEs move further from the corona through the interplanetary space (see G. P. Zank et al. 2015; O. V. Khabarova et al. 2016; J. A. le Roux et al. 2016; O. Khabarova et al. 2021; O. Malandraki et al. 2019). CME-associated charged particles accelerated to the MeV nuc^{-1} range may cause serious harm to sensitive equipment on board Earth-orbiting satellites and spacecraft in the interplanetary space, trigger a cascade of phenomena leading to a significant change in the global ionospheric electric circuit (I. A. Daglis et al. 2021; N. Buzulukova & B. Tsurutani 2022), and even pose threats to human safety (O. Khabarova et al. 2024).

On the one hand, the properties of the solar wind at the Earth's orbit are known to be mainly determined by low-latitude solar wind. In particular, the solar wind speed generally follows the number of sunspots below $+/-20°$ with respect to the solar equator (see Q. Jiao et al. 2023 and references therein). As a result, the scientific community is mostly interested in the CMEs associated with low-latitude active regions and directed toward the Earth, while CMEs at high apparent latitudes (ALs) are often treated as an unimportant part of space weather, having no consequences. The number of works discussing high-AL CMEs is relatively small (e.g., N. R. Sheeley et al. 1980; J. T. Gosling et al. 1995; J. Gosling & R. Forsyth 2001; D. B. Reisenfeld 2003; R. Von Steiger & J. D. Richardson 2006; C. Dumitrache et al. 2011; I. G. Richardson 2014; C. Scolini et al. 2020).

On the other hand, studying CMEs observed at high ALs in the solar corona is necessary for at least two reasons: (i) Investigating these phenomena helps elucidate the dynamics of solar magnetic fields and plasma and may bring important information on propagation of CMEs in the solar wind under specific conditions related to the open-field line shape of the solar magnetic field typical for heliolatitudes above $+/- 45°$ during solar minimum (but also occurring at lower latitudes during other phases of the solar cycle), and (ii) an interaction of high-AL CMEs with other CMEs, streams and flows may impact the propagation and geoeffectivennes of lower-latitude CMEs and stream interaction regions (SIRs).

In this study, we define high-AL CMEs as those detected within ±30° of the solar poles (e.g., E. Robbrecht et al. 2009). It is important to note that different research communities employ varying terminology for these events. In particular, they are sometimes referred to as CMEs with central position angles or principal angles (PAs) near the poles (e.g., A. Lara 2008; C. Shen et al. 2011) or as CMEs exhibiting high-latitude PAs observed (e.g., A. Lara 2008). In some statistical studies, they are simply termed high-AL CMEs (e.g., J. Lin et al. 2022). The tracking and modeling of CME propagation through the interplanetary space typically adopt a broader approach to CME localization, as these structures (representing sources of the high-speed solar wind) expand and influence extensive regions of the heliosphere.

The biggest attention to high-latitude ICMEs in the heliosphere was drawn after the Ulysses mission was launched (e.g., J. T. Gosling et al. 1995; J. Gosling & R. Forsyth 2001; D. B. Reisenfeld 2003; P. R. Gazis et al. 2006; W. B Manchester et al. 2006; I. G. Richardson 2014). Ulysses stands out as the sole spacecraft in human history to orbit the Sun nearly perpendicular to the ecliptic plane. Between 1990 and 2009, it provided invaluable data regarding the properties of interplanetary space across all heliolatitudes. Due to the absence of a coronagraph on board, understanding the ICME peculiarities detected by Ulysses at 2–3 au in the polar solar wind relies solely on the analysis of properties of the corresponding high-AL CMEs. There are several examples of comprehensive studies of such events that involve observing CMEs in the corona with terrestrial or near-terrestrial coronagraphs, case studies of the ICME parameters measured by Ulysses, and modeling the CME evolution from the Sun to Ulysses (e.g., I. G. Reisenfeld et al. 2003; C. Dumitrache et al. 2011).

Knowing properties of high-AL CMEs is important for studying solar activity, especially during the solar maximum phase (P. F. Chen et al. 2011), as well as for understanding associated space weather risks. High-AL CMEs are closely linked to so-called rush-to-the-poles phenomena in polar prominences, which signal the reversal of the solar global magnetic field (N. Gopalswamy et al. 2003, 2016). Polar prominence eruptions indicate the presence of large-scale bipolar magnetic fields that must cancel out before polarity reversals. Correspondingly, the associated high-AL CMEs facilitate the removal of bipolar regions from the Sun and complete the reversal process.

The morphology of high-AL CMEs is noticed to be different from that of low-AL ones. H. Cremades et al. (2020) have shown the so-called pancaking effect in high-AL CMEs determined by specific source region magnetic field configurations impacting the evolution of CME form and propagation characteristics from the very initial stages of their development. Their comprehensive multiviewpoint analysis of 12 high-AL CMEs has revealed asymmetrical expansion patterns, with higher speeds observed in the lateral direction compared to the axial direction below approximately 3 solar radii, impacting various aspects of CME morphology, shock generation, EUV wave formation, and related properties.

While moving in the coronal and solar wind ambient plasma, CMEs can change their expected path, suggesting expansion and radial propagation due to deflection and interaction with other structures. It is found that they can be deflected at the early stages of their propagation in the corona beyond two solar radii, i.e., very near to the Sun (Y. Wang 2014; C. Kay et al. 2017; J. Wang 2020; Y.-M. Wang & P. Hess 2023). This phenomenon is supposed to be linked to the ambient magnetic field configuration. CMEs are mostly deflected toward the heliospheric current sheet (HCS), and some of them are deflected toward pseudostreamers.

The combined numerical and observational evidence suggests that preexisting coronal flux ropes and pseudostreamers systematically influence early CME propagation by creating magnetic pressure gradients that steer eruptions away from a purely radial path (e.g., A. Sahade, et al. 2022; Y.-M. Wang & P. Hess, 2023; T. Török et al. 2024). CMEs originating near pseudostreamers tend to drift toward the pseudostreamer spine or low-energy corridors defined by the surrounding field, highlighting the role of large-scale coronal topology in shaping their trajectories. This implies that the presence and configuration of preexisting magneto-plasma structures can constrain CME evolution, affecting whether an eruption is deflected, guided, or partially confined (e.g., J. Wang et al. 2023).

The impact of the surrounding solar wind and large-scale magneto-plasma structures on ICMEs propagating through the heliosphere is comparable or even larger. For example, it was shown that an ICME can be significantly deflected by a stream from the long-lived coronal hole, which leads to an unexpected hitting the Earth with this geoeffective structure (O. V. Khabarova et al. 2016). The opposite situation is possible too, and, in combination with the near-Sun mechanisms, these are the main reasons why the Earth misses initially Earth-directed CMEs. Despite the obvious importance of this topic, there are not many studies dedicated to the interaction of CMEs with other magneto-plasma structures in the solar wind and their possible deflection resulting from this process (see N. Gopalswamy et al. 2009; N. Lugaz et al. 2017; M. J. Owens et al. 2017; Y. Shugay et al. 2018; N. Srivastava et al. 2018; S. J. Heinemann et al. 2019; E. Palmerio et al. 2021; M. Syed Ibrahim et al. 2022; P. Geyer et al. 2023, and references therein). Applying the results of the studies cited above to high-AL CMEs, one may suggest that such CMEs, although not hitting the Earth directly, may significantly impact other coexisting structures at lower latitudes, such as CMEs, SIRs, and the HCS, affecting their dynamics, properties, and geoeffectivennes. The notion concerning the role of high-latitude ICMEs in space physics remains largely unexplored in current literature, and investigating processes leading to CME/ICME deflection and interaction at varying heliocentric distances could significantly advance our understanding of space weather phenomena.

The number of CMEs at different latitudes varies over the 11 yr solar activity cycle. In particular, E. Robbrecht et al. (2009) showed the results of the comparative latitudinal analysis of the CME rate carried out for 1998 (minimum of the solar activity) and 2000 (maximum of the solar activity) based on the data from the Computer Aided CME Tracking software (CACTus) and Coordinated Data Analysis Workshop (CDAW) catalogs. Histograms for both databases peak at low ALs, but it is easy to find that the number of high-AL CMEs (CMEs detected at ALs above $+/-50^{\circ}$) drops dramatically during the minimum of the solar cycle and is comparable with that at the middle and low latitudes during the solar maximum. This tendency is confirmed by the analysis of ICMEs detected by heliospheric imagers on board the

STEREO mission (R. A. Harrison et al. 2018). Therefore, effects associated with high-AL CMEs cannot be ignored at least during the solar maximum, and more investigations are needed to analyze how their rate and characteristics change with time.

The primary objective of this research is to examine and compare statistical properties of high- and low-latitude-AL CMEs using extensive observational data from Solar and Heliospheric Observatory (SOHO) Large Angle and Spectrometric Coronagraph (LASCO) collected from 1996 to the end of 2025. We investigate variations in the quantity of CMEs and their characteristics, as well as propagation effects reflected in the Ulysses ICME detection rate. Additionally, as a discussion point, we underscore the significance of analyzing key CME features in combination with their initial development and propagation patterns in the corona, as well as the subsequent movement of ICMEs further from the Sun in the solar wind, to better understand their possible space weather effects. By comparing high and low-AL CMEs, we seek to understand how their properties vary with latitude and how these variations may affect the interplanetary medium as CMEs propagate away from the Sun. Differences in speed, width, and occurrence rates at various ALs can influence the global structure of the heliosphere, the timing and intensity of space weather events, and the impact of CMEs on planetary environments. At the same time, identifying consistent patterns across latitudes can help in characterizing typical CME behavior and improving models of solar activity.

2. Methods and Materials

To compile databases of high-LA CMEs that erupted within the $+/-30^{\circ}$ with respect to the poles and low-LA CMEs with the PAs lying within the $+/-30^{\circ}$ with respect to the solar equator and analyze their properties, we use data from LASCO on board SOHO (G. E. Brueckner et al. 1995). With two working coronagraphs, C2 and C3, LASCO provides images essential for tracking CMEs and knowing the characteristics of their spatial and temporal evolution.[4] SOHO is located at the first Lagrange point (L1), where the Sun–Earth gravity keeps it stable in orbit. In our statistical study, we mainly use the CDAW LASCO CME Catalog,[5] additionally employing the CACTus catalog[6] , as described below. We carry out a statistical analysis of the following parameters: the number of CMEs, the PA, the angular width, and the mean linear speed in 1996–2025. Note that the PA of each CME in our database of high-AL CMEs is calculated counterclockwise from the north.

Both the CDAW LASCO and CACTus catalogs are presented in the form of year-month tables. The CDAW LASCO CME catalog features CMEs manually identified since 1996 (N. Gopalswamy et al. 2010).[7] Each monthly list has details of CMEs along with the corresponding LASCO movies showing the evolution of structures in the corona. The "Remarks" column describes the CME quality from the movie, with an index notation (1–5) that indicates from poor to excellent with halo CME identification. We mostly rely on this

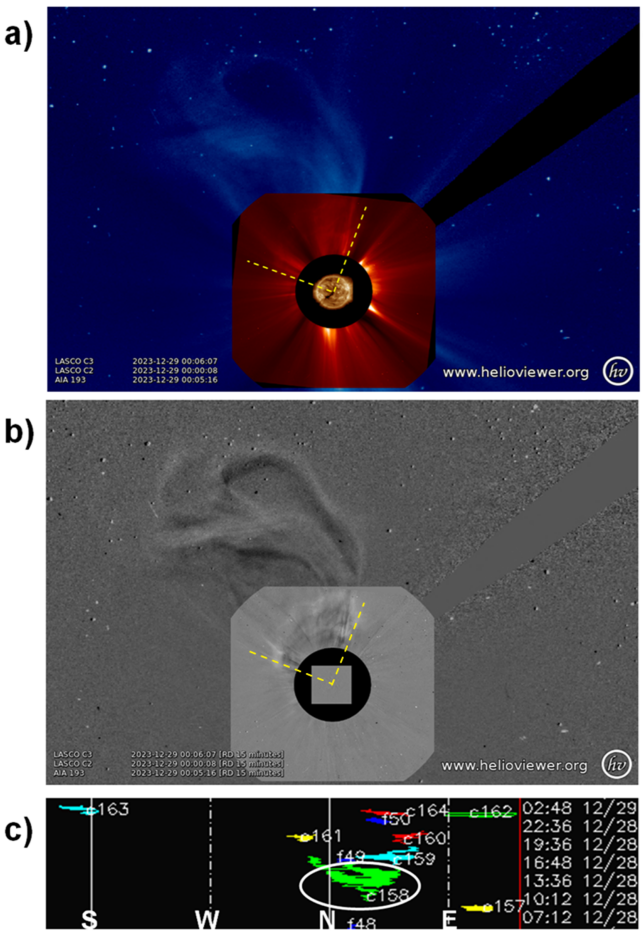

Figure 1. Example of the single CME observed at high latitudes in the solar corona. (a) Single CME ejected on 2023 December 29, composite image of SOHO LASCO C2 and C3 and Yohkoh SXT thin-Al. (b) Differential image of the same CME. (c) CACTUS catalog spatiotemporal map for the period corresponding to (a) and (b). E is for east, N means north, W stands for west, and S is south.

catalog since an expert's evaluation is known to give fewer errors than an automated detection of structures. The CDAW LASCO CME catalog covers the period from 1996 January 1 to 2025 November 30 (at the time of acceptance, no information on December 2025 CMEs was available), and CACTus provides the data from 1997 May 1 to 2025 December 31.

The CACTus catalog is based on the results of automatic identification of CMEs from LASCO's image sequences via the Hough transform by detecting motion of the brightest structures of CMEs (see E. Robbrecht et al. 2009).[8] One of the most useful features of CACTus is that CMEs detected in each month are shown not only in the form of a table but also in the map that visualizes useful information about the time and location of the ejections detected in the corona, marked by the stripe that corresponds to the angular width of each CME. In the spatiotemporal maps, north is indicated as N, W stands for the west, S corresponds to the south, and E means east. Note that W is on the right limb and E is on the left (W. T. Thompson 2006). An example of spatiotemporal CACTus maps can be found in Figure 1.

[4] See https://lasco-www.nrl.navy.mil/index.php?p=content/handbook/hndbk.

[5] http://cdaw.gsfc.nasa.gov/CME_list/index.html

[6] https://www.sidc.be/cactus/catalog.php

[7] Details on the procedure of CME identification and parameter measuring can be found at https://cdaw.gsfc.nasa.gov/CME_list/catalog_description.htm.

[8] See also https://www.sidc.be/cactus/about/index.html.

Each catalog has its own set of parameters of CMEs, which sometimes do not overlap. Owing to the methodological differences, the catalogs report a different number of CMEs, as CACTUS includes narrow or faint eruptions that may be omitted in the manual catalog, and may also subdivide a single manually identified CME into several detections, or, less frequently, merge features that a human observer would treat as separate events. An example of a single CME ejected on 2023 December 29 and recognized both manually in CDAW LASCO and automatically in CACTus is given in Figure 1. The LASCO images are obtained for illustrative purposes from Helioviewer.[9] In Figure 1(a), the single high-AL CME from the CDAW CME catalog is shown. The corresponding differential image in Figure 1(b) allows for visually distinguishing CME edges with confidence. The particular CME has a classic shape with the twisted flux rope and clearly seen borders indicated by dashed lines in Figure 1(a), according to which it is easy to measure the angular width of the particular CME. The spatiotemporal CACTus map mentioned above is shown in Figure 1(c). It indicates the exact location of the ejection in the case of the single CME (see the oval next to N).

Coronagraphic PA reflects the apparent angular location of a CME in the plane of the sky and does not directly correspond to its true heliographic latitude. This discrepancy arises from both projection geometry and the seasonal variation of the solar B-angle. A CME launched at any heliographic latitude but originating near the central meridian (Stonyhurst longitude $\approx 0^{\circ}$) will experience reduced projection distortion compared with limb events, although its observed PA still does not uniquely determine the true latitude. For CMEs originating closer to the limb, the plane-of-sky PA can differ substantially from the actual ejection latitude, and midlatitude CMEs may be observed with PAs near 0° or 360°, giving the appearance of high-latitude eruptions. These projection effects are systematic and do not fully cancel in statistical samples (e.g., L. A. Balmaceda et al. 2018; C. Verbeke et al. 2022); for instance, projected widths tend to be overestimated and projected speeds underestimated (J. T. Burkepile et al. 2004). Despite these limitations, our study uses the same projected LASCO-derived parameters as prior long-term CME statistical analyses, allowing direct comparison with earlier results. Because our focus is on broad solar-cycle trends rather than on recovering true CME latitudes or deprojected kinematics, the use of PA-based measurements remains appropriate for identifying large-scale statistical behavior, even though individual values may deviate from their true heliographic counterparts.

We extract dates and parameters of the single and halo CME events from the LASCO catalog, filtering each by PA ($+/-30^{\circ}$ with respect to the pole or equator) and the quality index. The movies of every complex and halo event are checked by eye. The level zero CACTus catalog (until 2015 October) and the quick-look CME list (from 2015 November until 2025 November) are used to check the angular width, the PA, and the linear speed of the CMEs. Halo CMEs contribute to the total CME number calculations but do not contribute to the statistics of low- and high-AL CMEs. After compiling the database, a statistical analysis of the parameters listed above is carried out to show the properties of CMEs over the solar cycle. We compare the behavior of the parameters in different phases of the solar cycle and analyze the trends, plotting both distributions of the parameters and comparative figures. Talking about the phases of the 11 yr solar cycle, we use the following selection of periods: (i) solar activity minimum years: 1996 May–1997 December, 2008 January–2009 December, and 2019 December—2021 February ; (ii) maximum: 2000 March–2002 February, 2013 November–2015 March and 2023 December—December 2025; (iii) rising phase: 1997 January–2000 February, 2010 January–2013 October, 2021 March–2022 December; (iv) declining phase: 2002 March–2007 December and 2015 April–2019 November.

While comparing the number of CMEs in the corona with ICMEs observed by the Ulysses spacecraft at the same latitudes during the same period, we checked whether Ulysses projection was on the proper side of the limb, and the corresponding delay for the CME propagation from the Sun to Ulysses, which sometimes may be a week or longer, was taken into account.

3. Results

3.1. Rate and Spatial Characteristics of CMEs

Figure 2(a) presents the yearly number of CMEs observed by SOHO LASCO over two and a half solar cycles. Green indicates all CMEs listed in the CDAW catalog, while the red curve represents the annual rate of CMEs covering all latitudes as reported in CACTus over the same period. Figures 2(b) and (c) show the number of low- and high-AL CMEs, respectively, with full-halo CMEs removed. Figure 2(d) displays the number of CMEs identified in the corona alongside the number of ICMEs observed in situ by the Ulysses spacecraft. For the CDAW LASCO catalog, high-AL CMEs are shown in yellow and low-AL CMEs in light blue. For ICMEs detected by Ulysses, high- and low-AL events are shown in green and blue, respectively. Figure 2(e) illustrates the solar cycle through daily and yearly averaged sunspot numbers.

The CME rate is known to be different in different catalogs, but the general trends remain very similar (e.g., S. Yashiro et al. 2008; E. Robbrecht et al. 2009; Ph. Hess & R. C. Colaninno 2017; P. L. Lamy et al. 2019). The correlation analysis between the annual CME rates and sunspot numbers reveals a dependence on AL. High-AL CMEs exhibit a stronger correlation with the solar cycle than low-AL ones, with Pearson coefficients of 0.727 (CDAW) and 0.704 (CACTus). Low-AL CMEs show weaker correlations, 0.645 (CDAW) and 0.596 (CACTus). Considering all CMEs irrespective of latitude, the total counts also correlate strongly with sunspot numbers, with coefficients of 0.758 (CDAW) and 0.663 (CACTus), suggesting that the CACTus catalog may include a larger proportion of events with less reliable detection.

Figure 2(d) further compares the number of high- and low-AL CMEs ejected from the Sun with the number of corresponding ICMEs detected by Ulysses at high and low heliolatitudes during the same period. Although Ulysses measurements cover a shorter interval compared to the full dataset in Figure 2, they provide valuable insights into the propagation of CMEs to distances beyond 1 au. It is evident that the number of ejected high- and low-AL CMEs was several times larger than the number of ICMEs detected by Ulysses, while CMEs ejected during solar minimum were more likely to reach Ulysses. The red curve in Figure 2(d) indicates the maximum ratio of CDAW LASCO high- and

[9] https://helioviewer.org/

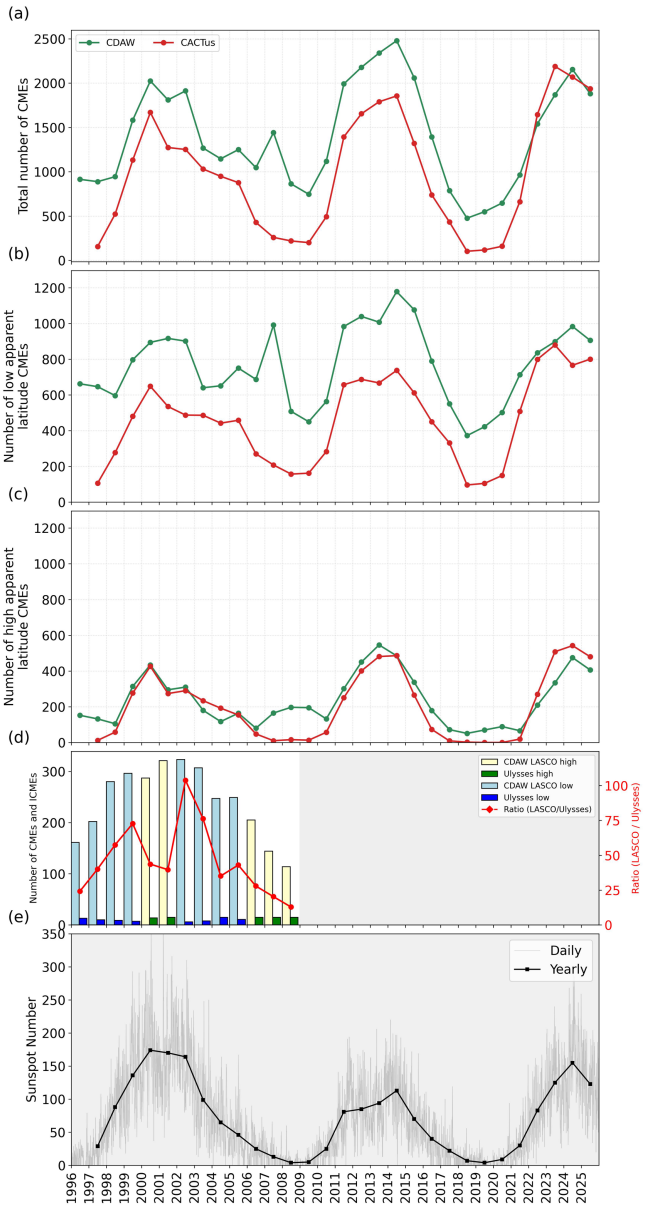

Figure 2. Number of CMEs per year vs. sunspot number from 1996 to 2023. (a) Total number of all CMEs listed in CDAW (green) and CACTUS (red) catalogs. (b) Low-AL CMEs indicated in both catalogs. (c) High-AL CMEs vs all CMEs indicated in both catalogs. (d) Number of low-AL (light blue) and high-AL (yellow) CMEs observed by LASCO vs the number of ICMEs detected by the Ulysses spacecraft in the solar wind at high heliolatitudes (green) and low heliolatitude (blue). The red curve shows the ratio of the LASCO CME number to the ICME number. The gray area corresponds to the period during which Ulysses did not provide observational data. (e) Sunspot number. Light gray is for daily data, and black is for the yearly average.

low-AL CMEs to the number of Ulysses ICMEs, observed near the solar maximum.

The Ulysses ICME number curve is shifted by one year relative to the LASCO curve, and the maximum correlation with sunspot numbers (0.98) is achieved with a two-year shift. These results demonstrate that both CME and ICME rates are strongly modulated by the solar cycle. The optimal time shifts indicate that Ulysses ICMEs exhibit a phase delay in their solar-cycle pattern relative to sunspot numbers, whereas LASCO high- and low-AL CMEs remain closely synchronized with solar activity near the Sun, reaching a correlation coefficient of 0.98 with only a one-year delay. This suggests that the more complex interplanetary medium during solar maximum, with coexisting SIRs, coronal hole flows, and propagating ICMEs, has a stronger impact on CME propagation to several heliocentric distances.

The number of manually identified CMEs in the CDAW catalog is generally larger than the number of automatically recognized CMEs in the CACTus, according to Figure 2(a), and it is stably larger for low-AL CMEs, while the numbers are almost the same for high-AL CMEs. Note that Figure 2(a) differs from the results of the previous statistical studies (e.g., S. Yashiro et al. 2008) because today's CACTus Version 2 catalog is cleared out of poor and mistakenly identified events. It is easy to see that, for example, in the previous version (Version 1 catalog),[10] 93 events are identified in 2007 January versus only 38 CMEs listed in the Version 2 catalog in the same month. Therefore, the results of all previous statistical studies employing the CACTus CME Version 1 catalog should be considered with caution because, in contrast with the modern Version 2 catalog, they include properties of poor events and non-CME events.

Considering different phases of the solar cycle separately, it is easy to find that the relatively high correlation of the high-AL CME number with the sunspot number is mainly determined by two phases of the cycle. Figures 3 and 4 show monthly numbers of low-AL CMEs (Figure 3) and high-AL CMEs (Figure 4) from the CDAW catalog versus the monthly averaged sunspot number. The red color of the dots corresponds to the solar minimum, deep blue—to the solar maximum, green—to the rising, and cyan—to the declining phase. The number of CMEs in both figures follows the variation in sunspot numbers more closely during the rising and declining phases of the solar cycle. The corresponding correlation coefficients are consistently higher for high-AL CMEs than for low-AL CMEs. The increase in correlation when longer averaging windows are used suggests that sunspot activity acts primarily as a long-term modulating factor rather than an immediate driver of CME rates. This implies that additional processes, operating on shorter timescales or involving different regions of the solar atmosphere, contribute to the variability in CME occurrence at both high and low ALs.

3.2. PA

Figure 5 shows the distribution of PAs over the two and a half solar cycles in the form of a polar histogram, where events are categorized into three distinct AL regions based on their PA. These categories, high-AL CMEs (red), low-AL CMEs (blue), and mid-AL CMEs (gray), are plotted against four distinct solar-cycle phases, similar to Figure 4. Event counts are derived from the CDAW/LASCO catalog (1996–2025), binned in 10° segments, and displayed with a common radial limit to enable direct visual comparison of event magnitudes by phase and region. Note that in solar terminology, the right side is west and the left is east.

It is easy to see how the number and spatial distribution of the events vary over the solar cycle. Although the low-AL events always dominate, the general form of the spatial distribution changes with the solar cycle. In particular, during the solar minimum, there are two distinct picks of events,

[10] Still available at https://www.sidc.be/cactus/scan/scan.html.

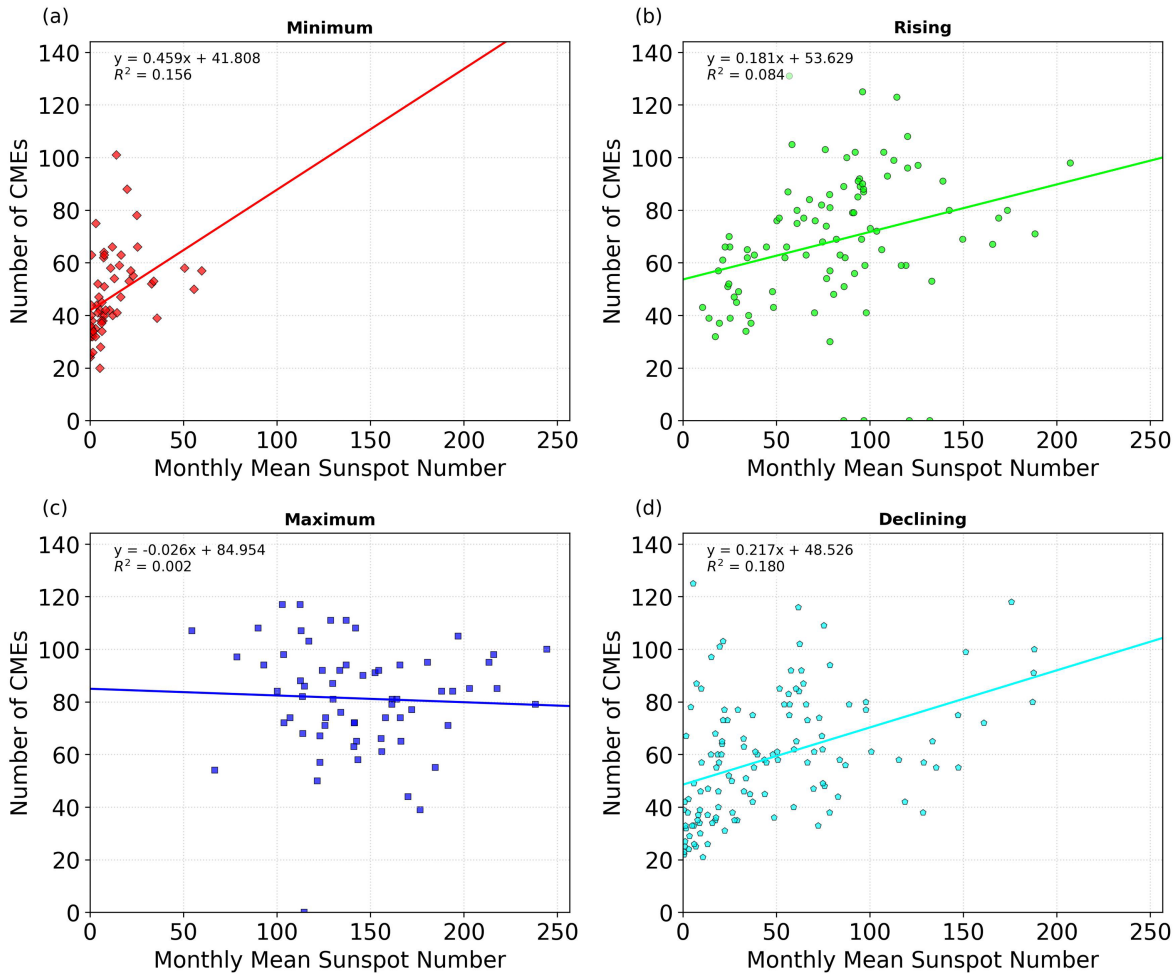

Figure 3. Monthly rate of low-AL CMEs vs. sunspot number for four phases of the 11 yr solar activity cycle. (a) Minimum, (b) rising, (c) maximum, and (d) declining phase of solar activity.

around the poles and the equator, while during the other phases of the solar cycle, the mid-AL events fill the gap and make the view smoother. During the solar maximum, the low-AL CMEs are erupted with a slight shift to the south, and during the rising phase, their distribution is skewed with respect to the equator to the north on the western side and to the south on the eastern side. During the declining phase, the tendency is the opposite. There is a general tendency of high-AL CMEs to prevail in the north across all phases of the solar cycle except during the solar maximum.

3.3. Linear Speed and Angular Width

The yearly averaged linear speed and the angular width of CMEs are calculated on the basis of both the CDAW and CACTus catalogs (Figure 6). The CME speed slightly varies with distance in the corona, but the height-time dependence generally remains linear; therefore, the linear speed in CDAW is considered as one of the important parameters allowing predicting further dynamics of a particular CME. Using it, one can also estimate the kinetic energy that a CME brings into the heliosphere. Figure 6 illustrates the relationship between CME properties and solar activity. Panels (6a) and (6b) show the variations in mean linear speed and the angular width of all CMEs, respectively, as a function of the sunspot number, indicated with blue. Data from the CDAW (green) and CACTus (gray) catalogs are shown. Solar-cycle dependencies are clearly evident in the CDAW data, whereas the CACTus data exhibit weaker correlations. The raw correlation coefficients at zero lag are 0.848 (CDAW) and 0.447 (CACTus) for speed, and 0.799 (CDAW) and 0.713 (CACTus) for angular width.

Panels (6c) and (6d) present the speed and angular width of low- and high-AL CMEs from the CDAW catalog only, with low-AL CMEs in blue and high-AL CMEs in red. Both speed and width follow the solar cycle, but low-AL CME speeds correlate more strongly with sunspot number ($r = 0.842$) than high-AL CME speeds ($r = 0.502$), consistent with the closer association of low-latitude CMEs with sunspots. The angular width correlation is similar for low- and high-AL CMEs (0.760 and 0.754, respectively), and shows slight improvement when a one-year negative lag is applied. This indicates that changes in CME width precede solar-cycle variations, suggesting potential predictive applications.

4. Discussion and Conclusions

This study investigates the statistical properties of CMEs over two and a half solar cycles (1996–2025) using data from the SOHO/LASCO CDAW and CACTus catalogs. The results reveal distinct behaviors for low- and high-AL CMEs, emphasizing the critical role of high-AL CMEs in

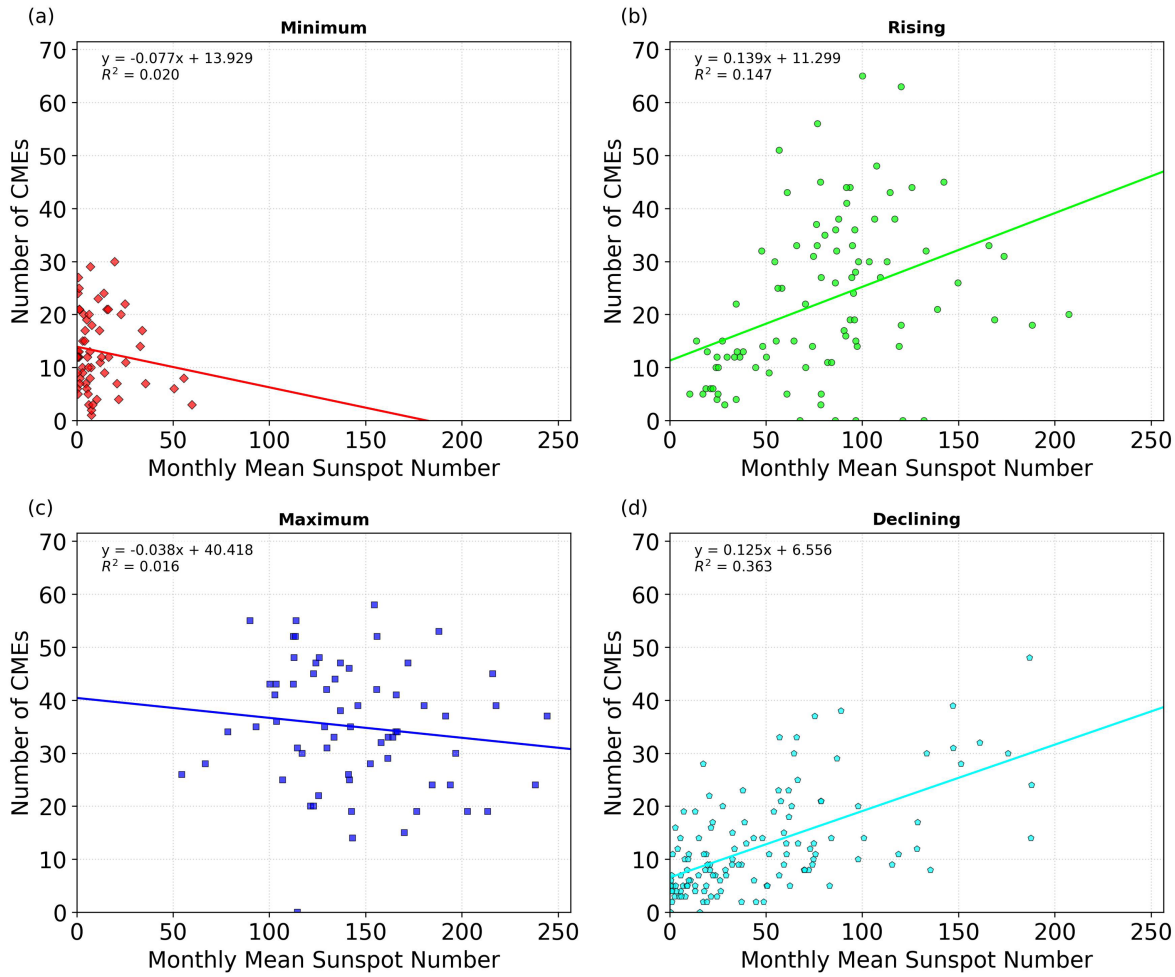

Figure 4. Analogous to Figure 3, but for the monthly rate of high-AL CMEs.

characterizing CME dynamics across the solar cycle and their complex propagation through the heliosphere. CMEs are well-recognized drivers of severe space weather, posing risks to both space-based and ground-based technologies. The CME-associated solar wind periods at Earth's orbit exhibit a strong correlation with the solar cycle (K. Mursula et al. 2022); therefore, CMEs represent the biggest threat during solar maxima. Such risks extend to out-of-ecliptic missions, underscoring the need to understand properties and dynamics of both low- and high-AL CMEs. The other reason to study high-AL CMEs is their impact on the propagation of lower-latitude geoeffective ICMEs and flows from coronal holes.

Determining CME position angles from single-view coronagraph images is inevitably affected by projection effects, which can shift the AL from the true heliographic latitude, particularly for eruptions away from the plane of the sky or near the Sun–observer line. These distortions depend on both CME direction and observing geometry (M. Skirgiello 2003; J. T. Burkepile et al. 2004; T. A. Howard et al. 2008; E. Robbrecht et al. 2009), which is why CME catalogs report ALs instead of heliolatitudes. Strongly projected events can mix with weakly projected ones, complicating the interpretation of apparent-latitude distributions and preventing reconstruction of true latitudes. Nevertheless, long-term statistical analyses remain meaningful when interpreted in terms of relative behavior and cycle-dependent variations. The CDAW and CACTus catalogs provide internally consistent AL measurements over nearly three solar cycles, allowing general trends in CME occurrence and large-scale properties to be reliably identified. In this study, ALs are used with the understanding that they include unavoidable projection uncertainties, but they are suitable for comparative and long-term analyses, even if they do not reflect true CME latitudes.

Due to the radial expansion of CMEs, any event observed as ejected within $\pm 30^\circ$ of the pole will extend further into polar directions as it propagates outward. This means that even if an event is initially misclassified due to projection effects, its physical extent will eventually cover high latitudes in the heliosphere, making most misidentifications negligible in terms of CME heliospheric impact. Studies confirm that CME angular widths increase with distance from the Sun, especially up to 0.4 au, and their expansion leads to broader coverage of heliospheric latitudes (e.g., C. Scolini et al. 2021; F. N. Minta et al. 2023). The impact of initial positional errors on statistical results is rather low, reinforcing that statistical trends, rather than absolute values, remain the most significant aspect of studies of CME apparent properties. Indeed, despite the exact values of the CME rate varying from catalog to catalog, the corresponding trends are found to be very similar both in our study and prior works (e.g., S. Yashiro et al. 2008; E. Robbrecht et al. 2009; Ph. Hess & R. C. Colaninno 2017; P. L. Lamy et al. 2019).

Knowing variations in the CMEs' number, direction, angular width, and linear speed is crucial for CME modeling,

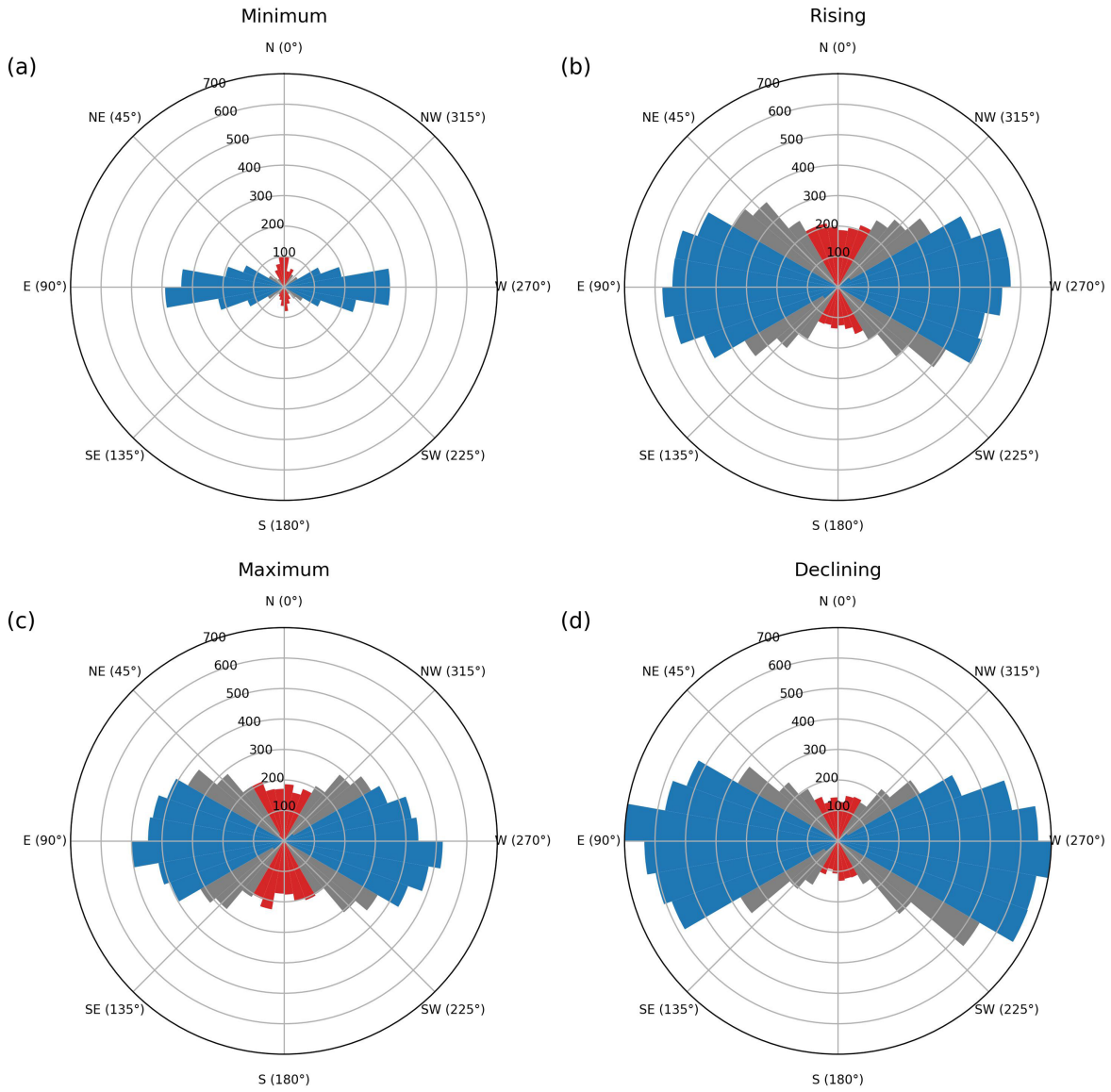

Figure 5. PA distribution of CMEs by solar-cycle phase. The polar histogram shows the frequency distribution of CMEs from the CDAW/LASCO catalog across four solar-cycle phases: (a) minimum, (b) rising, (c) maximum, and (d) declining phase. The radial axis represents the event count. Three distinct angular regions are categorized and plotted: high-AL CMEs (red), low-AL CMEs (blue), and mid-AL CMEs (gray). The angular axis is oriented with north (N) at 0° and proceeds clockwise (standard PA).

and understanding their solar-cycle behavior enhances space weather prediction across all heliolatitudes. While prior studies have explored similar topics, their primary focus has been on low-latitude CMEs or the general properties of all CMEs. The results of our study indicate that the solar-cycle modulation of CME activity depends on the AL. For example, the number of high-AL CMEs shows a stronger correlation with the solar cycle than that of low-AL ones, and this difference likely reflects both physical and observational factors. High-AL CMEs mostly originate from active regions that evolve with the solar cycle, while low-AL CMEs can also come from quiet-Sun filaments or regions outside major active regions, which introduces more variability in their occurrence. Projection effects and detection biases near the equator may also impact the result.

One might assume that the number of high-AL CMEs simply reflects the corresponding number of sunspot groups at high latitudes. However, the latter peaks approximately one year before the solar-cycle maximum and declines more rapidly (K. Li et al. 2000), while the yearly rate of high-AL CMEs follows the solar cycle much better. This discrepancy arises because not all active regions are associated with ejections. In particular, it has been found that the number of high-AL CMEs follows the coronal brightness index with a higher correlation coefficient than the same parameter at latitudes below 50° (J. Lin et al. 2022).

The linear speeds of all CMEs and ICMEs observed in the solar wind at all heliolatitudes are known to follow the solar cycle well (e.g., D. Barnes et al. 2019), and ICMEs tend to be wider during solar maximum (R. A. Harrison et al. 2018). This illustrates the necessity to study the physical processes lying behind such behavior of high-AL CMEs. In particular, unusual polar conditions observed in Cycle 24 (Gopalswami et al. 2016b; V. N. Obridko et al. 2024) could affect the statistical properties of high-AL CMEs, which differ from typical ones of CMEs at lower latitudes.

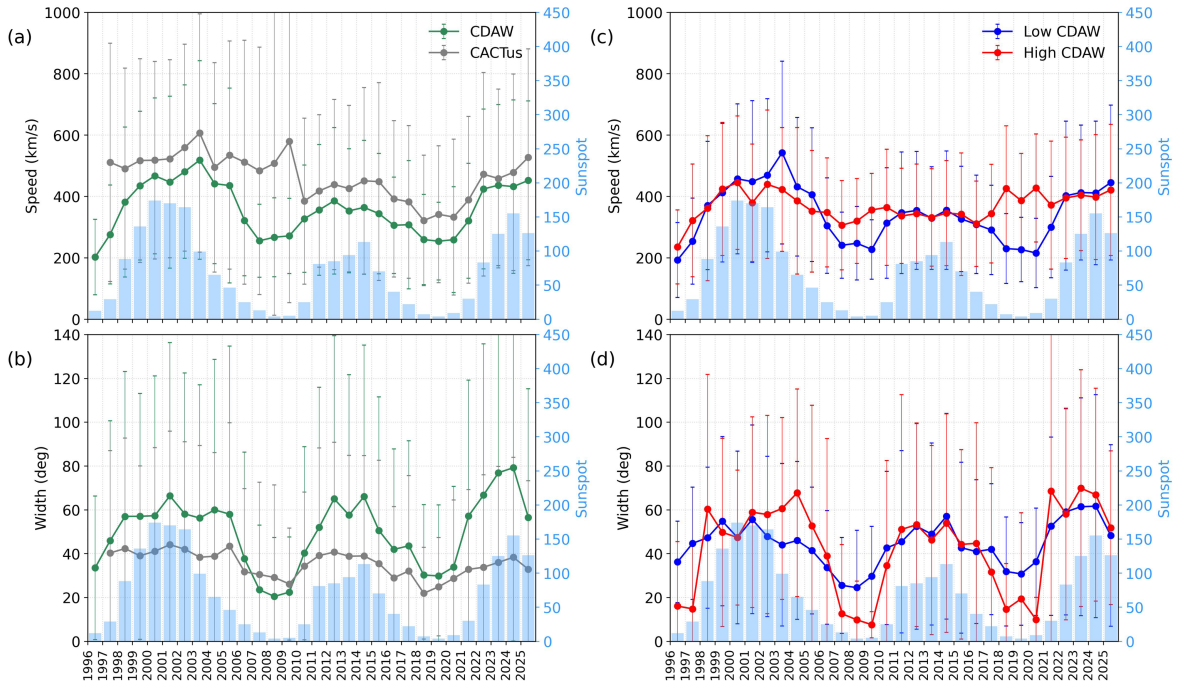

Figure 6. Linear speed and angular width from two LASCO catalogs vs sunspot number. CDAW LASCO catalog data are marked in green, and CACTus data are red. (a) Yearly averaged value of the CME speed, all ALs. (b) Yearly averaged angular width, all ALs. (c) Yearly averaged value of the CME speed for low- and high-AL CMEs, CDAW data. (d) Yearly averaged angular width, for low- and high-AL CMEs, CDAW data. The yearly averaged number of sunspots is given in light blue in each panel for comparison.

Our results confirm that CME propagation in the heliosphere is strongly modulated by the solar cycle. Propagation effects reduce the number of ICMEs at Ulysses during solar maximum, but the long-term solar-cycle pattern remains clear. The number of CMEs observed at the Earth is known to be smaller than that observed in the corona and initially directed toward the Earth, and the tendency remains the same at any point at ~1 au (e.g., D. Barnes et al. 2020). As discussed in the Introduction, this may be a result of deflection of CMEs that occurs at any stage of their propagation and their interaction with the surrounding solar wind, streams, flows, and the HCS. For the Ulysses dataset, the correlation with sunspot numbers at zero time shift is relatively low because not every CME observed near the Sun is later detected by Ulysses. During propagation, CMEs can be deflected, decelerated, or distorted by the solar wind and by interactions with other CMEs. These effects are found to be stronger during solar maximum, when the solar wind is more variable, and CMEs are more frequent, increasing the likelihood that some CMEs do not reach Ulysses. Introducing a time shift of 2 yr raises the correlation to almost 100%, indicating that ICME occurrence at Ulysses closely follows the solar cycle, with a systematic phase offset relative to sunspot activity.

An interesting fact is that during the solar minimum, more ICMEs were detected by Ulysses than during solar maximum. Knowing that high-AL CMEs are generally narrower during the minimum of the solar activity, one may suggest that the CME-insufficiency effect observed during the high solar activity is mainly determined by peculiarities of CME propagation, but not their width. A preliminary analysis of observations of the high-AL CMEs enhanced by PFSS modeling of magnetic fields in the corona, ENLIL modeling, and observations with heliospheric imagers or interplanetary scintillations (see O. V. Khabarova et al. 2016, O. Khabarova et al. 2021), shows that high-AL CMEs propagating along open magnetic field lines may follow the surrounding topology of magnetic fields if their source is located near coronal holes. This is often the case for CMEs observed at high AL near the solar minimum and at middle latitudes in other phases of the solar cycle. Taking into account the previously noted peculiarities of high-AL CMEs discussed in the Introduction, one can conclude that some CMEs can be significantly deflected from the original direction of their propagation due to the coexistence with coronal holes in the nearest vicinity of the ejection region.

One of the bright examples of such events is the recent CME detected on 2023 June 21, 09:36:07, with the PA 34° and the linear speed 949 km s^{-1}, according to the CDAW LASCO catalog (Figure 7). There are significant discrepancies in the estimation of properties of such CMEs in different catalogs because of their unusual form. In particular, CACTus detected this CME as a part of halo-IV CME with the median linear speed 1249 km s^{-1}, which occurred at 10:12 and combined with a flow; while the Space Weather Database of Notifications, Knowledge, Information (DONKI)[11] shows it at 09:48 with the speed 773 km s^{-1} and a comment on the asymmetry of its leading edge and complicated fitting with a model. Figure 7 illustrates the reason for these complications reflected in coronagraph images from STEREO Ahead (Figure 7(a)) and LASCO (Figure 7(b)). The particular ejection that occurred on 2023 June 21 has an unusual skewed form, which makes it difficult to model and even recognize the CME with automated methods. Figure 7(c) shows observations of the Solar Dynamics Observatory (SDO) in the 21.1 nm wavelength, picturing the conditions in the lower corona in the early post-eruption period. Besides active regions, there are three small

[11] https://kauai.ccmc.gsfc.nasa.gov/DONKI/view/CME/25651/1

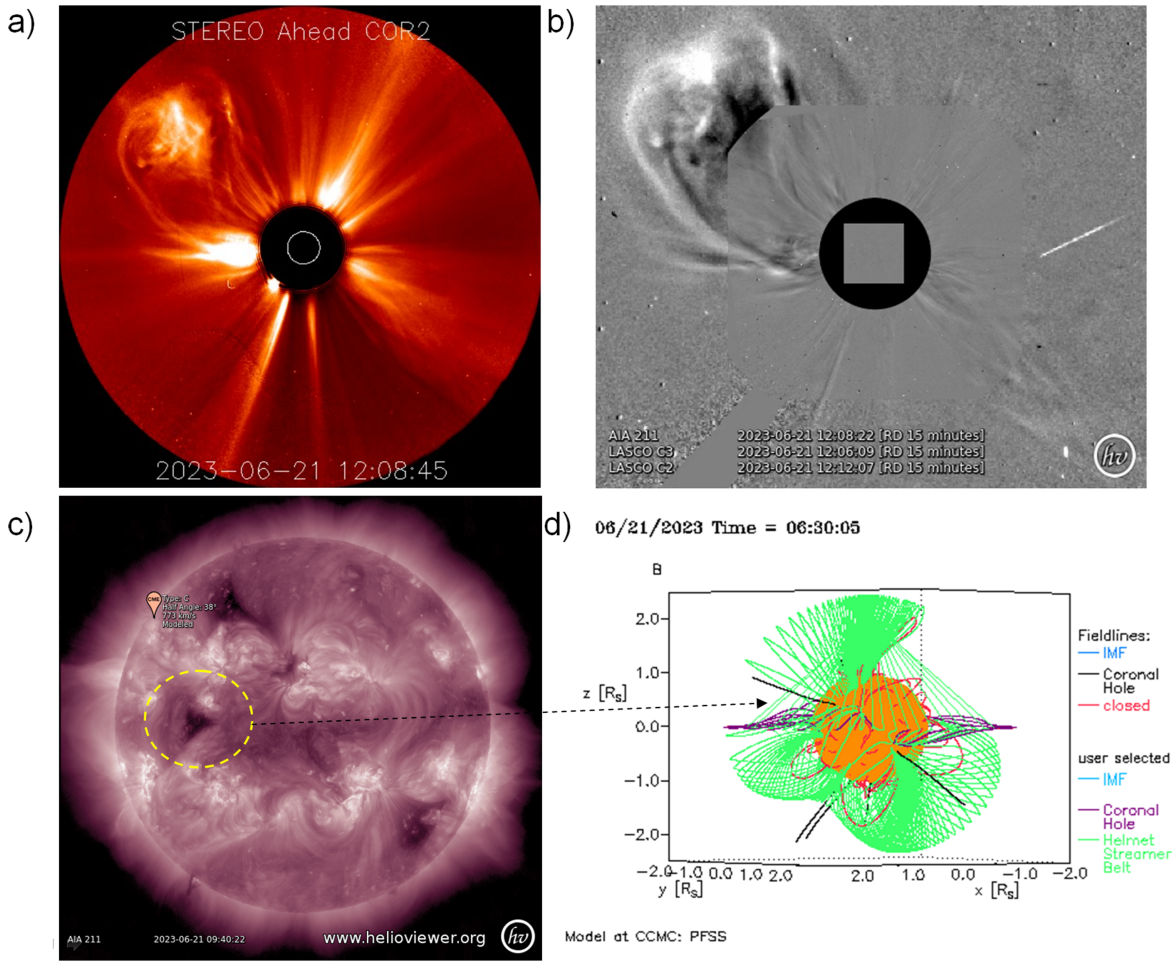

Figure 7. Example of the elephant-trunk CME, deflected in the corona because of the coexistence with the flow from the coronal hole. (a) Image of the CME obtained from STEREO A COR2 on 2023 June 21 (animation of this figure is available at https://cdaw.gsfc.nasa.gov/stereo/daily_movies/2023/06/21/index.html); (b) SOHO LASCO observations of the same event, differential image; (c) location of the CME (provided by DONKI) and the coronal hole indicated by the yellow dashed circle in the SDO AIA 211A image; (d) modeled magnetic field line topology in the corona. CME propagates in the open-field line area shown with the arrow, along the black open-field line indicating the edge of the coronal hole between the coronal hole magnetic field (purple) and the helmet streamer belt field (green) lines.

coronal holes on the disk, one of which impacted the CME propagation (indicated by the circle). The corresponding large-scale topology of the magnetic field lines in the corona seen in Figure 7(d) is reconstructed with the Potential Field Surface (PFSS) model and can be found at the Integrated Space Weather Analysis system website.[12]

On the one hand, the flow from the coronal hole at low latitudes did not allow the CME to propagate freely in the corona and pushed it toward higher latitudes, determining its elephant-trunk form, and, on the other hand, while propagating in the interplanetary space, the CME expansion deflected the coronal hole flow toward the lower heliolatitudes. One can find from the ENLIL modeling results that the particular CME merges with the SIR at the coronal hole flow border further in the inner heliosphere, and its in-ecliptic part hits Mars.[13]

Therefore, although the PA of this CME is positioned at a lower AL, which would typically classify it as a middle-latitude event, its skewness toward higher latitudes results in a scenario where, at greater distances from the Sun, this CME may be detected as a high-latitude event. Such events, where a CME is initially observed at lower latitudes but exhibits skewness toward higher latitudes at greater distances from the Sun, are relatively poorly studied and not well understood. The dynamics of CMEs, particularly those with unusual spatial distributions, present significant challenges for both observational techniques and theoretical modeling. The interaction between solar wind conditions, magnetic field configurations, and the propagation of the CME through the heliosphere is complex, and these events are not well-represented in current models.

This lack of understanding is compounded by the difficulty in distinguishing the behavior of CMEs at varying latitudes, especially as they propagate from the Sun and interact with the interplanetary medium. Given the potential for these events to impact space weather phenomena, such as geomagnetic storms, understanding their behavior and predicting their evolution is crucial. Further study is needed to refine models that account for the latitudinal skewness of CMEs and to improve observational techniques that can detect such phenomena at varying heliocentric distances. This would enhance our ability to forecast space weather events and

[12] https://iswa.ccmc.gsfc.nasa.gov/IswaSystemWebApp/?layout=PFSS
[13] https://iswa.gsfc.nasa.gov/downloads/20230621_141300_2.0_anim.timden.gif

mitigate their potential effects on satellite systems, communication infrastructure, and space missions.

Summarizing: the statistical analysis of CMEs at high and low ALs across two and a half solar cycles (1996–2025) yielded distinct characteristics modulated by solar activity and propagation effects in the heliosphere.

1) The occurrence rate of CMEs is strongly correlated with the solar cycle. However, the strength of this correlation varies with latitude.
   a. The total yearly number of CMEs exhibits the strongest correlation with the sunspot number, compared with the numbers of high-AL CMEs and low-AL CMEs. In turn, the yearly rate of high-AL CMEs demonstrates a stronger correlation with the solar cycle than the rate of low-AL ones.
   b. The correlation between monthly CME rates and sunspot activity is consistently higher for both high-AL and low-AL CMEs during the rising and declining phases of the solar cycle. The increase in the correlation with increasing timescales (from months to years) suggests that the solar activity reflected in sunspot numbers functions primarily as a long-term modulating factor, not capturing local processes responsible for the CME rate.
2) The study identified a strong, solar-cycle-dependent variation in the number of CMEs erupted from the corona compared to ICMEs detected in situ by the Ulysses spacecraft.
   a. The number of both high- and low-AL CMEs observed in the corona was several times larger than the number of ICMEs detected by Ulysses. The variation of the ejected/detected ratio is strongly dependent on solar activity, as CMEs ejected during solar minimum were more likely to reach Ulysses than those ejected during solar maximum. This low detection efficiency during solar maximum is most probably attributed to the more complex interplanetary medium, which increases the likelihood of deflection and interaction of CMEs with other large-scale magneto-plasma structures.
   b. ICME occurrence at Ulysses follows the solar cycle with a systematic phase offset of approximately two years relative to sunspot activity.
3) An analysis of the spatial characteristics of CMEs shows that, while low-AL CMEs consistently dominate in number, the distribution of CMEs by eruption direction changes over the solar cycle.
   a. Two distinct peaks in the number of CMEs appear during solar minimum: one at low and one at high ALs, with a gap in between.
   b. High-AL CMEs are found to be directed preferentially to the north during the minimum, rising, and declining phases of the solar cycle, showing south–north asymmetry.
   c. At solar maximum, low-AL CMEs show a slight southward bias. During the rising phase, they are northward on the western side and southward on the eastern side, with the opposite pattern in the declining phase.

   The patterns may be affected by the hemispheric asymmetry.
4) Kinematic and spatial properties for CMEs exhibit varying degrees of correlation with the solar cycle based on AL. The linear speed and the angular width of both low-AL and high-AL CMEs follow the solar cycle. The linear speed of low-AL CMEs correlates more strongly with the sunspot number than the speed of high-AL CMEs.
5) The correlation for angular width is similar for low-AL and high-AL CMEs in following the solar cycle, and its variations precede the sunspot number variations, which may be used for prognostic purposes.
6) We note that the new, improved CACTus catalog differs significantly from the previous version, so earlier statistical studies based on it should be interpreted with caution.

The results of this statistical study can be applied to modeling high-speed solar wind associated with CMEs at both high and low heliolatitudes. They highlight the critical importance of understanding magnetic field topology and conditions at the time of CME eruption, as well as propagation effects, such as CME–CME interactions and interactions with surrounding streams and flows, in shaping the evolution of high-AL CMEs beyond the corona. These findings underscore the need for further studies of the impact of high-AL CMEs on space weather. To bridge the existing gaps in our understanding of the dynamic processes associated with these powerful magneto-plasma structures, further investigation through case studies of in situ observations in the heliosphere, complemented by advanced modeling, is essential.

Acknowledgments

This study was carried out as part of the activity of the Space Weather Center of Tel Aviv University (https://www.spaceweather.sites.tau.ac.il/). O.K.'s work is partially supported by the European Union (STORM project, GA No. 101223119 STORM).

Data Availability

The number of sunspots is obtained from the GSFC/SPDF OMNIWeb interface at https://omniweb.gsfc.nasa.gov/form/dx1.html. LASCO coronograph data are available at https://lasco-www.nrl.navy.mil/index.php?p=content/database. We thank providers and scientists working to compile the CDAW LASCO CME catalog (http://cdaw.gsfc.nasa.gov/CME_list/index.html), CACTus catalog (https://www.sidc.be/cactus/catalog.php), and DONKI space weather activity catalog (https://kauai.ccmc.gsfc.nasa.gov/DONKI/search/). SOHO LASCO images are from Helioviewer.org (https://helioviewer.org/), part of the Helioviewer open-source project for the visualization of solar and heliospheric data funded by ESA and NASA. Results of the PFSS model (Janet Luhmann's code) are from the ISWA website (https://iswa.ccmc.gsfc.nasa.gov/IswaSystemWebApp/?layout=PFSS). The Ulysses spacecraft data are from the Ulysses Final Archive (https://ufa.esac.esa.int/ufa/)

ORCID iDs

Olga Khabarova https://orcid.org/0000-0002-3230-2033
Colin Price https://orcid.org/0000-0002-1387-7632

References

Balmaceda, L. A., Vourlidas, A., Stenborg, G., & Dal Lago, A. 2018, ApJ, 863, 57
Barnes, D., Davies, J. A., Harrison, R. A., et al. 2019, SolPhys, 294, 57
Barnes, D., Davies, J. A., Harrison, R. A., et al. 2020, SolPhys, 295, 150
Besliu-Ionescu, D., & Mierla, M. 2021, FrASS, 8, 79
Brueckner, G. E., Howard, R. A., Koomen, M. J., et al. 1995, SolPhys, 162, 357
Burkepile, J. T., Hundhausen, A. J., Stanger, A. L., St. Cyr, O. C., & Seiden, J. A. 2004, JGRA, 109, 3103
Buzulukova, N., & Tsurutani, B. 2022, FrASS, 9, 1017103
Chen, P. F. 2011, LRSP, 8, 1
Cremades, H., Iglesias, F. A., & Merenda, L. A. 2020, A&A, 635, A100
Daglis, I. A., Chang, L., Dasso, S., et al. 2021, AnnGeo, 39, 1013
Dumitrache, C., Popescu, N. A., & Oncica, A. 2011, SolPhys, 272, 137
Gazis, P. R., Balogh, A., Dalla, S., et al. 2006, in Coronal Mass Ejections. Space Sciences Series of ISSI, ed. H. Kunow et al., 21 (Springer)
Geyer, P., Dumbovic, M., Temmer, M., et al. 2023, A&A, 672, A168
Gopalswamy, N. 2016, GSL, 3, 8
Gopalswamy, N., Mäkelä, P., Xie, H., et al. 2009, JGR, 114, A00A22
Gopalswamy, N., Shimojo, M., Lu, W., et al. 2003, ApJ, 586, 562
Gopalswamy, N., Yashiro, S., & Akiyama, S. 2016, ApJL, 823, L15
Gopalswamy, N., Yashiro, S., Michalek, G., et al. 2010, Sun&Geo, 5, 7
Gosling, J., & Forsyth, R. 2001, SpSciRev, 97, 98
Gosling, J. T., Bame, S. J., Mccomas, D. J., et al. 1995, SpSciRev, 72, 133
Harrison, R. A., Davies, J. A., Barnes, D., et al. 2018, SolPhys, 293, 77
Heinemann, S. G., Temmer, M., Farrugia, C. J., et al. 2019, SolPhys, 294, 121
Hess, Ph., & Colaninno, R. C. 2017, ApJ, 836, 134
Howard, R. A., Vourlidas, A., & Stenborg, G. 2003, FrASS, 10, 1264226
Howard, T. A., Nandy, D., & Koepke, A. C. 2008, JGRA, 113, A01104
le Roux, J. A., Zank, G. P., Webb, G. M., & Khabarova, O. V. 2016, ApJ, 827, 47
Jiao, Q., Liu, W., Zhang, D., & Cao, J. 2023, ApJ, 958, 70
Kay, C., Gopalswamy, N., Xie, H., & Yashiro, S. 2017, SolPhys, 292, 78
Khabarova, O., Malandraki, O., Malova, H., et al. 2021, SpSciRev, 217, 38
Khabarova, O., Pinaev, S. K., Chakov, V. V., et al. 2024, FrPH, 12, 1295643
Khabarova, O. V., Zank, G. P., Li, G., et al. 2016, ApJ, 827, 122
Kilpua, E., Koskinen, H. E. J., & Pulkkinen, T. I. 2017, LRSP, 14, 5
Lamy, P. L., Floyd, O., Boclet, B., et al. 2019, SpSciRev, 215, 39
Lara, A. 2008, ApJ, 688, 647
Li, K., Gu, X., Xiang, F., et al. 2000, MNRAS, 317, 897
Lin, J., Wang, F., Deng., L., et al. 2022, ApJ, 932, 62
Lugaz, N., Temmer, M., Wang, Y., & Farrugia, C. J. 2017, SolPhys, 292, 64
Malandraki, O., Khabarova, O., & Bruno, R. 2019, ApJ, 881, 116
Manchester, W. B., IV, & Zurbuchen, T. H. 2006, JGR, 111, A05101
Minta, F. N., Nozawa, S., Kozarev, K., Elsaid, A., & Mahrous, A. 2023, JASTP, 247, 106080
Mursula, K., Qvick, T., Holappa, L., & Asikainen, T. 2022, JGR, 127, e2022JA030830
Obridko, V. N., Shibalova, A. S., & Sokoloff, D. D. 2024, SolPhys, 299, 60
Owens, M. J., Lockwood, M., & Barnard, L. A. 2017, SciRep, 7, 4152
Palmerio, E., Nieves-Chinchilla, T., Kilpua, E. K. J., et al. 2021, JGR, 126, e2021JA029770
Reames, D. V. 2021, Solar Energetic Particles. Lecture Notes in Physics, 978 (Springer)
Reisenfeld, D. B. 2003, JGR, 30, 8031
Richardson, I. G. 2014, SolPhys, 289, 3843
Robbrecht, E., Berghmans, D., & Van der Linden, R. A. M. 2009, ApJ, 691, 1222
Sahade, A., Cécere, M., Sieyra, M. V., et al. 2022, A&A, 662, A113
Scolini, C., Chané, E., Pomoell, J., Rodriguez, L., & Poedts, S. 2020, SpWea, 18, e2019SW002246
Scolini, C., Dasso, S., Rodriguez, L., Zhukov, A. N., & Poedts, S. 2021, A&A, 649, A69
Sheeley, N. R., Jr, Howard, R. A., Koomen, M. J., Michels, D. J., & Poland, A. I. 1980, ApJ, 238, L161
Shen, C., Wang, Y., Gui, B., Ye, P., & Wang, S. 2011, SoPh, 269, 389
Shugay, Y., Slemzin, V., Rodkin, D., Yermolaev, Y., & Veselovsky, I. 2018, JSWSC, 8, A28
Skirgiello, M. 2003, GeoRL, 30, 1995
Srivastava, N., Mishra, W., & Chakrabarty, D. 2018, SolPhys, 293, 5
Von Steiger, R., & Richardson, J. D. 2006, Coronal Mass Ejections. Space Sciences Series of ISSI, 21 (Springer)
Syed Ibrahim, M., Uddin, W., Joshi, B., Chandra, R., & Kumar Awasthi, A. 2022, RAA, 21, 318
Thompson, W. T. 2006, A&A, 449, 791
Török, T., Linton, M. G., Leake, J. E., et al. 2024, ApJ, 962, 149
Verbeke, C., Schmieder, B., Démoulin, P., et al. 2022, AdSpR, 70, 1663
Wang, J., Hoeksema, J. T., & Liu, S. 2020, JGR, 125, e2019JA027530
Wang, J., Siqing, L., & Bingxian, L. 2023, AdvSpRes, 72, 5263
Wang, Y.-M., & Hess, P. 2023, ApJ, 952, 85
Wang, Y., Wang, B., Shen, C., Shen, F., & Lugaz, N. 2014, JGRA, 119, 5117
Yashiro, S., Michalek, G., & Gopalswamy, N. 2008, AnnGeo, 26, 3103
Zank, G. P., Hunana, P., Mostafavi, P., et al. 2015, ApJ, 814, 137